Hindawi
Advances in Materials Science and Engineering
Volume 2022, Article ID 2207585, 11 pages
https://doi.org/10.1155/2022/2207585

Research Article

Steel Wire Mechanical Property Degradation Study Based on Numerical Simulation

Jiangjiang Li [1,2] and Xuanyu Zhang [3]

[1] *School of Highway, Chang'an University, Xi'an, Shaanxi 710064, China*
[2] *Middle Section of the South Second Ring Road, Xi'an, Shaanxi 710064, China*
[3] *Shandong Hi-Speed Company Limited, Long'ao North Road, Jinan, Shandong 250000, China*

Correspondence should be addressed to Jiangjiang Li; lijiangjilin@chd.edu.cn

Received 8 March 2022; Revised 8 April 2022; Accepted 11 April 2022; Published 9 June 2022

Academic Editor: REN Fuqiang

With the rapid development of underground engineering construction, such as deep mining of mineral resources and tunnel excavation under complex geological conditions, the existing support methods cannot meet the deformation requirements. It is necessary to conduct in-depth research on the stress status and damage evolution of the hanger rods, to establish a theoretical basis for the design principles and criteria of key components. In this paper, the degradation law of the mechanical properties of the hanger steel wire with the degree of corrosion is analyzed in detail. The results show that the corrosion changes the geometry of the cross section of the steel wire, which leads to the degradation of the mechanical properties of the steel wire. With the increase of corrosion length and depth, the strength, stiffness, and ultimate strain of the steel wire are reduced to varying degrees, and the effect of pitting corrosion is more significant than that of uniform corrosion. The closer the holes are, the greater the corrosion effect is.

1. Introduction

Since the 1980s, with the development of large-scale highway and urban construction, the construction of highways and urban bridges, mining of mineral resources, and excavation of tunnels have been greatly developed in our country [1–5]. Steel wire is commonly used in many engineering fields, such as tunnel excavation, underground space structure, and so on [6, 7]. According to the "2006 Statistical Bulletin on the Development of Highway and Waterway Transportation Industry" of the Ministry of Communications, by the end of 2006, the total number of highway bridges in China had reached 533,600, with a total of 20,399,100 meters, including 1,036 extra-large bridges, 1,714,500 meters, and 30,982 bridges, 6,385,800 meters. There are 121,100 middle bridges, but the cross-section is still circular [8–10]. A large number of representative world-class bridges have been built over the Yangtze River, Yellow River, Pearl River, and other major rivers and coastal waters.

However, with the rapid development of bridge construction in China, the destruction of bridges during construction or operation also occurs from time to time, resulting in heavy casualties and property losses, as well as extremely bad social impacts. Among the bridge damage accidents in the past ten years, the middle and bottom-bearing arch bridges are the worst. Among them, the bridge decks of the Yibin Nanmen Bridge in Sichuan (Figure 1(a)) and the Xinjiang Kongque River Bridge (Figure 1(b)) collapsed in 2001 and 2011, respectively.

From the analysis of the existing accident causes, in addition to factors such as construction, material quality, and overloading, another important reason is the lack of a deep enough understanding of the structural mechanical behavior and damage mechanism of middle and bottom-bearing arch bridges [11–17]. Based on the ANSYS finite element software, this study simulates the effects of uniform corrosion and pitting corrosion on the mechanical properties of the steel wire and analyzes the degradation law of the mechanical properties of the steel wire under different

(a) (b)

Figure 1: Damage forms of different bridge decks.

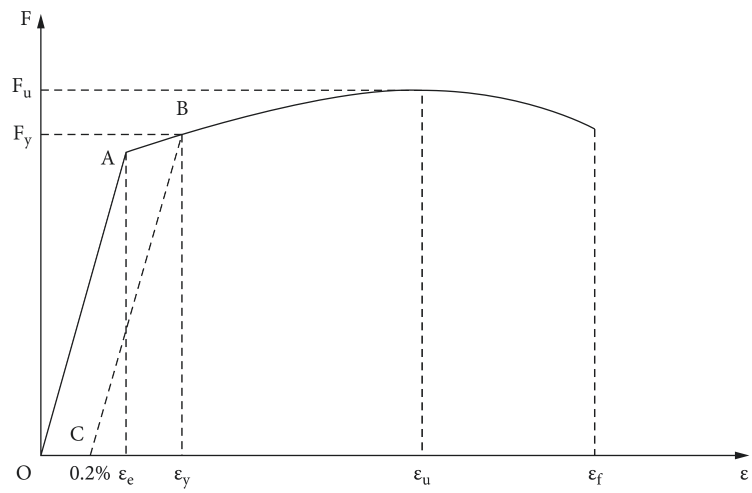

Figure 2: F-ε curve of steel wire and the mechanical meaning of each symbol.

corrosion depths or lengths [18]. Before discussing the degradation law of the mechanical properties of the steel wire with the degree of corrosion, the symbols in this study are explained in Figure 2 [19–23].

2. Stress-Strain Relationship of Damaged Steel Wire

With the increase of corrosion degree, the mechanical properties such as stiffness, strength, and ultimate strain of steel wire will be reduced to different degrees. After analyzing the results of tensile tests of damaged steel wires, Elachachi et al. proposed the following constitutive relation [24]:

$$\begin{cases} \sigma = Ee, & 0 < \varepsilon \leq E_e, \\ E - \sigma_e + \dfrac{E(\varepsilon - \varepsilon_e)}{1 + C(\varepsilon - \varepsilon_e)}, & \varepsilon \leq \varepsilon \leq \varepsilon_f, \end{cases} \tag{1}$$

where $c = E\varepsilon L_u - \sigma_u/(\sigma_u - \sigma_e)(\varepsilon_u \varepsilon_e)$.

In order to study the degradation law of mechanical properties of steel wire, Xu [25] conducted corrosion detection and monotonic tensile tests on damaged steel wires. Two data reflecting the corrosion degree of steel wire are obtained by testing: the average diameter d_{mean} (reflects the average corrosion degree of steel wire specimens) and the minimum diameter $d_{\min}$ (reflects the local corrosion degree of the steel wire specimen). Also, four mechanical performance parameters of each damaged steel wire including yield bearing capacity F_y, yield strain ε_y, ultimate bearing capacity F_u, and ultimate strain ε_y were measured by tensile tests. It can be seen from the test results that the constitutive relation of each damaged steel wire basically conforms to equation (1). The force-strain curves of some steel wires under different corrosion grades are plotted in Figure 3.

It can be seen that with the increase of the degree of corrosion, the mechanical properties such as stiffness, strength, and ultimate strain of the steel wire are reduced to varying degrees. The changing law is shown in Figures 4(a)–4(e).

It can be seen from Figure 4 that the axial stiffness of the steel wire decreases nonlinearly with the increase of the corrosion degree. There is an approximately linear relationship between yield capacity and ultimate capacity and minimum diameter. When $d_{\min}$ changed from 5.00 mm to 2.94 mm, F_y decreased from 29.06 kN to 15.15 kN, a decrease of 47.87%; F_u decreased from 33.41 kN to 17.28 kN, a decrease of 48.28%. The ultimate strain ε_u decreases linearly with the decrease of the minimum diameter $d_{\min}$ of the steel

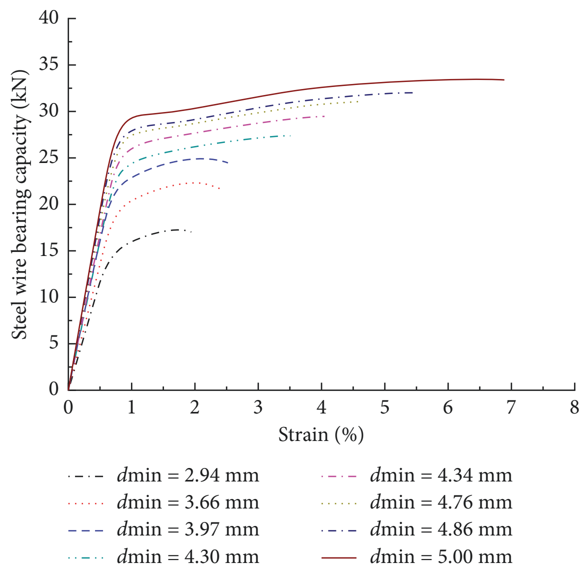

Figure 3: Bearing capacity-strain curve of damaged steel wire.

wire, and the relationship between the two can be approximated by an exponential function, as shown in the following equation:

$$\varepsilon_u = 1.9591 + 3.43542 \times 10^{-4} e^{d\min/0.52505}. \quad (2)$$

3. Establishment of Finite Element Model of Damaged Steel Wire

Both uniform corrosion and pitting corrosion change the cross-sectional geometry of the steel wire, but their contributions to the brittle fracture of the steel wire are not the same. Uniform corrosion uniformly reduces the area of the cross section of the wire, but the cross section is still circular and it only changes the cylindrical shape of the wire in the longitudinal direction. The local pitting corrosion changes the cross section of the steel wire due to the formation of local corrosion pits on the surface of the steel wire, so that the cross section changes from circular to noncircular. The authors in [26–29] pointed out that the ultimate ductility of high-strength steel wire is determined by the geometry of the steel wire, and the change of the cross-sectional geometry of the steel wire is determined by the degree of uniform corrosion and pitting corrosion. When the geometry of the longitudinal cylinder of the steel wire changes due to uniform corrosion, the ultimate ductility of the steel wire decreases, and the fracture originates at the center of the cross section and then spreads to the outer surface. When corrosion holes are formed on the surface of the steel wire, the ultimate ductility of the steel wire decreases more, and the fracture originates from the deepest corrosion hole on the surface of the steel wire.

Corrosion not only results in a reduction in the ductility of the wire but also results in a reduction in its strength and stiffness. The authors in [26, 30, 31] only considered ductility reduction when simulating steel wire corrosion, and their research conclusions need to be further expanded. On the basis of that research, this section also considers the influence of ductility reduction, strength reduction, and stiffness reduction of steel wire to study and discuss the degradation law of the mechanical properties of damaged steel wire in the section of the boom.

3.1. Defining Model Types, Element Types, and Material Properties. The steel wire adopts SOLID45 three-dimensional solid element, and the yield criterion adopts von Mises yield criterion [32]. According to this yield criterion, the critical shear stress of the steel wire under uniaxial tension is taken as $\sigma_y/3$ (σ_y is the yield stress of the wire).

3.2. Establishing a Steel Wire Model. The finite element model was first established with intact steel wire, with a length of 25.4 cm and a diameter of 4.877 mm. The corrosion section is located in the middle section of the steel wire and has a length of 5 mm. The steel wire can be divided into 16 segments longitudinally, and the dimensions are 4×31.115 mm + 8×0.625 mm + 4×31.115 mm. Among them, the middle 8 sections are used to simulate uniform corrosion and pitting corrosion. The cross section of the steel wire is composed of the following parts: (1) 16 square units in the middle with an area of 1.016 mm × 1.016 mm; (2) 4 inner rings to the outer diameter of 2.131 mm; (3) 6 intermediate rings to an outer diameter of 2.371 mm; and (4) 8 outer rings to the 2.438 mm outer diameter. In the model, 8 outer rings are used to simulate uniform corrosion, and 6 middle rings are used to simulate pitting corrosion. The geometric model and meshing of the steel wire are shown in Figure 5, and the total number of elements is 9216.

3.3. Simulation of Corrosion in the Model. In the finite element model of steel wire, the stress concentration at the crack tip is ignored, and the change of material properties caused by hydrogen embrittlement is not considered. Using the accelerated corrosion test data of high-strength steel wire in the literature [26], that is, the uniform corrosion rate of 0.0838 μm/h, the pitting corrosion rate is taken as 0.3848 μm/h. To analyze the effect of pitting pits and irregularities in the geometry of the wire section, 4 different corrosion conditions were simulated:

(1) A, uniform corrosion and pitting corrosion in the direction of 0° of the cross section.
(2) B, uniform corrosion and pitting corrosion in the direction of 0° and 90° of the cross section.
(3) C, uniform corrosion and pitting corrosion of 0° and 90° of the cross section.
(4) D, uniform corrosion + pitting corrosion at 3 points of 0°, 45°, and 90° of the cross section.

The solid model of the steel wire does not consider the large strain property, and the material nonlinearity adopts the multilinear isotropic strengthening stress-strain relationship MISO. The ultimate strain of the steel wire is taken as 5.7%, and all elements whose strain exceeds the ultimate strain are passivated, that is, multiplying their stiffness by

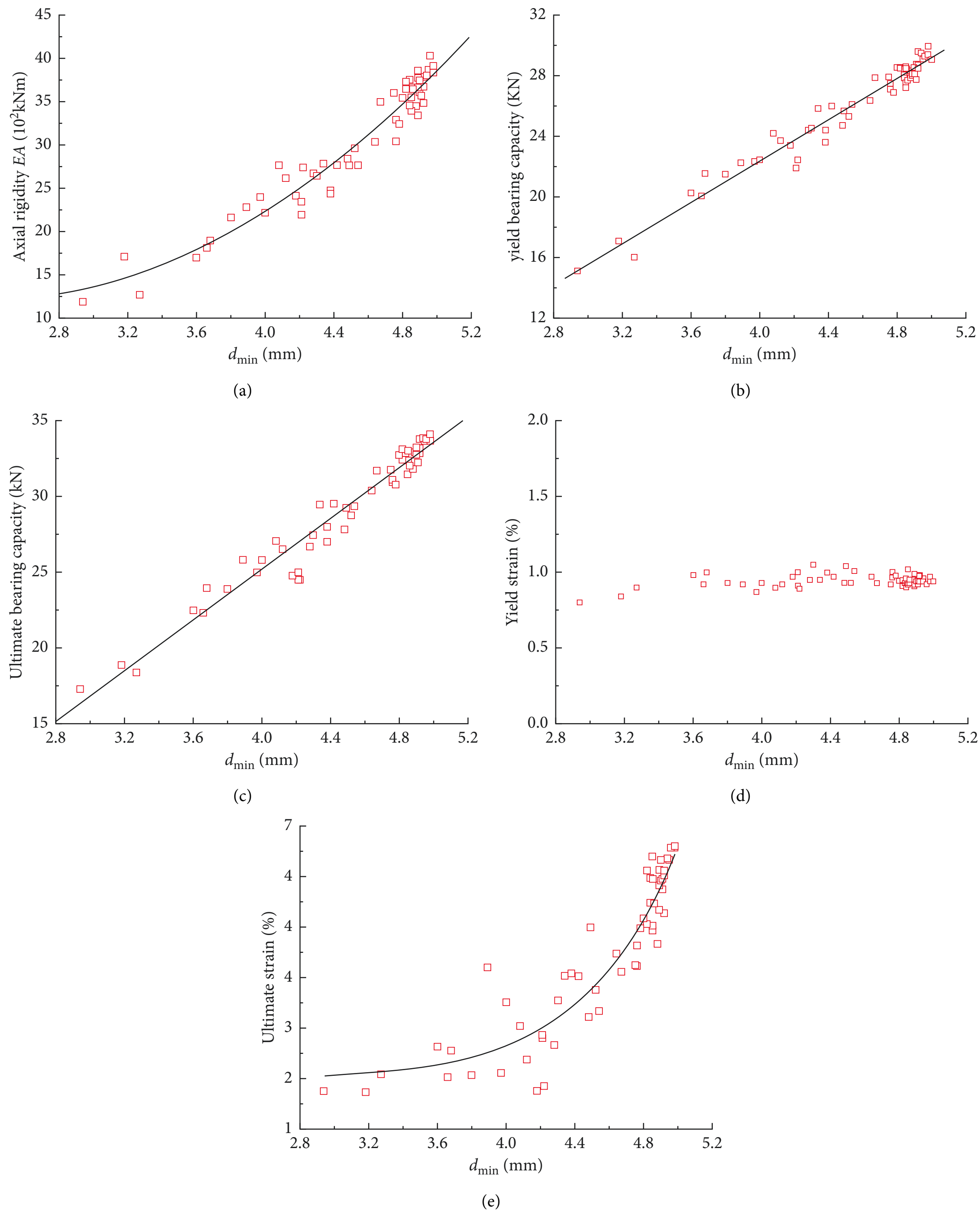

Figure 4: Change law of different mechanical parameters. (a) Axial stiffness degradation. (b) Yield bearing capacity degradation. (c) Deterioration of ultimate bearing capacity. (d) Yield strain degradation. (e) Ultimate strain degradation.

1.0×10^{-5}. When the nonlinear solution converges, if no element is passivated, the end displacement is increased by 0.01 and the solution is continued; if any element is passivated, the end displacement is not increased and the solution is continued. This cycle is repeated until the whole wire breaks.

4. The Effect of Uniform Corrosion on the Mechanical Properties of Steel Wire

The uniform corrosion conditions of different corrosion lengths and depths were simulated, respectively (32 models in total), and the ultimate strain of the steel wire under each

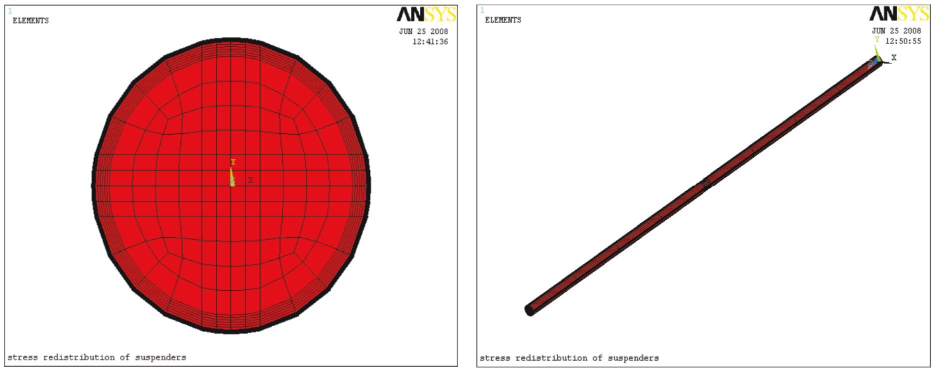

Figure 5: Wire model and meshing diagram.

Table 1: Ultimate strain of steel wire under uniform corrosion.

Corrosion time (h)	Corrosion length (mm)	Corrosion depth (mm)	Ultimate strain	Corrosion time (h)	Corrosion length (mm)	Corrosion depth (mm)	Ultimate strain
100	1.25	0.008	0.046	500	1.25	0.042	0.041
	2.50	0.008	0.045		2.50	0.042	0.038
	3.75	0.008	0.044		3.75	0.042	0.037
	5.00	0.008	0.044		5.00	0.042	0.033
200	1.25	0.017	0.045	600	1.25	0.05	0.039
	2.50	0.017	0.044		2.50	0.05	0.036
	3.75	0.017	0.043		3.75	0.05	0.034
	5.00	0.017	0.042		5.00	0.05	0.031
300	1.25	0.025	0.043	700	1.25	0.059	0.037
	2.50	0.025	0.042		2.50	0.059	0.034
	3.75	0.025	0.041		3.75	0.059	0.032
	5.00	0.025	0.038		5.00	0.059	0.029
400	1.25	0.034	0.043	800	1.25	0.067	0.036
	2.50	0.034	0.04		2.50	0.067	0.033
	3.75	0.034	0.038		3.75	0.067	0.031
	5.00	0.034	0.036		5.00	0.067	0.027

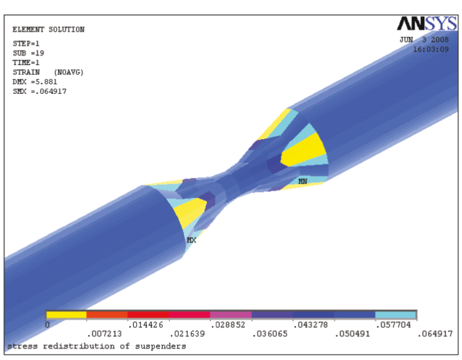

Figure 6: "Cup-cone" fracture of the uniformly corroded steel wire.

working condition is shown in Table 1. The data show that the ultimate strain of steel wire not only decreases with the extension of the uniform corrosion length but also decreases with the increase of the uniform corrosion depth. When the steel wire is intact, the fracture type is a cup-cone fracture (see Figure 6); when the steel wire is uniformly corroded, the fracture originates from the center of the wire and then expands outward, with the fracture retaining the cup-cone shape.

4.1. Influence of Uniform Corrosion Depth on Mechanical Properties of Steel Wire. Under the condition of uniform corrosion at different depths, the evolution law of mechanical properties of steel wire is shown in Figures 7 and 8.

It can be clearly seen from Figures 7 and 8 that when the uniform corrosion depth of the steel wire gradually develops from 8.38 (100 h) to 0.067 mm (800 h), the ultimate strain of the steel wire decreases nonlinearly, from 0.046 to 0.027, but the reduction in the strength and stiffness of the steel wire is not significant. At the same time, with the increase of the uniform corrosion depth, the cross section of the steel wire becomes smaller, and its cross section shape is still circular. Because the brittle fracture of the steel wire is greatly affected by the change of the geometric shape of the steel wire cross section, the brittle fracture mechanism of the steel wire does not change under the condition of uniform corrosion at different depths, and it all originates from the center of the steel wire cross section, which is a cup-cone fracture.

4.2. Influence of Uniform Corrosion Length on Mechanical Properties of Steel Wire. Under the condition of uniform corrosion of different lengths, the evolution law of mechanical properties of steel wire is shown in Figures 9 and 10.

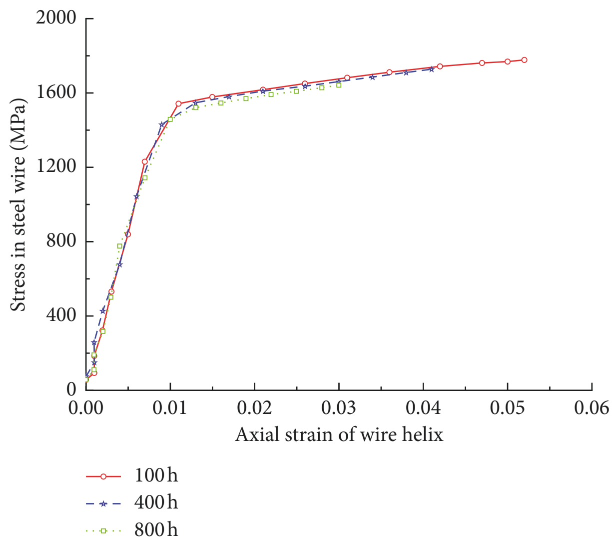

FIGURE 7: Effect of uniform corrosion depth on mechanical properties of steel wire.

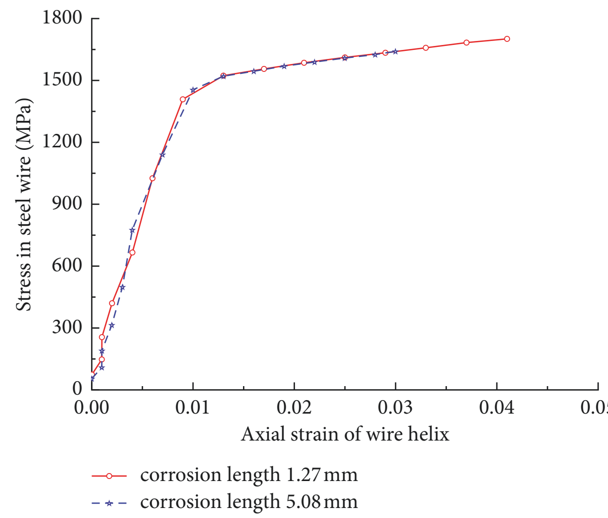

FIGURE 9: Effect of uniform corrosion depth on mechanical properties of steel wire.

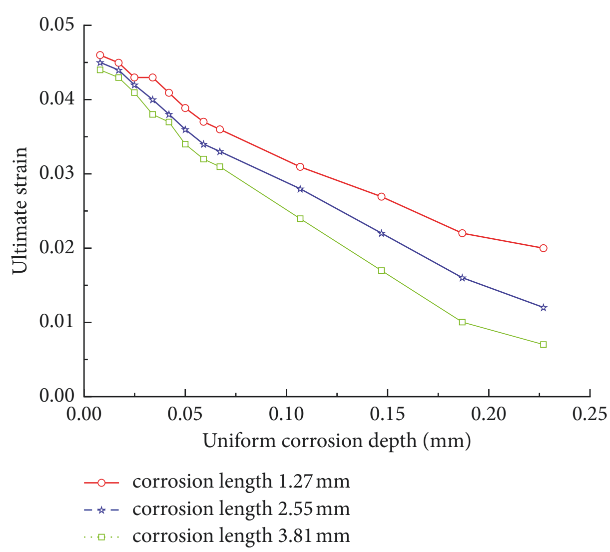

FIGURE 8: Influence of uniform corrosion depth on ultimate strain of steel wire.

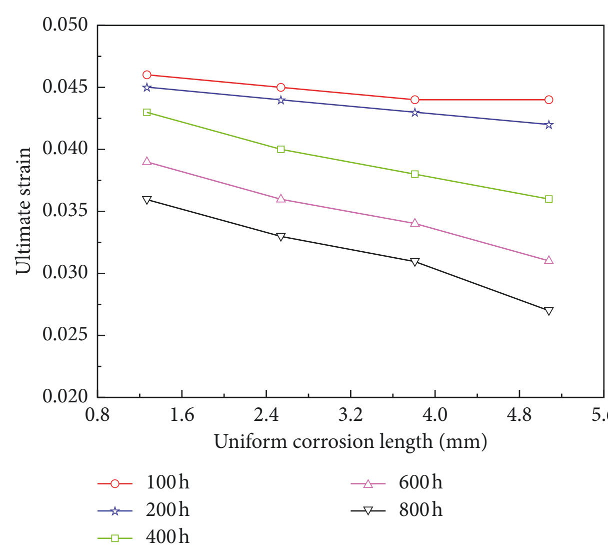

FIGURE 10: Influence of uniform corrosion depth on ultimate strain of steel wire.

It can be seen from the figures that when the uniform corrosion length of the steel wire gradually develops from 1.25 mm to 5.00 mm, the ultimate strain of the steel wire basically decreases linearly. Compared with the effect of corrosion depth, under the condition of uniform corrosion of different lengths, the reduction in strength and stiffness of steel wire is less obvious.

5. Influence of Pitting Corrosion on Mechanical Properties of Steel Wire

Table 2 shows the simulation results of the ultimate strain of the steel wire under different length and depth pitting corrosion conditions. The results show that the mechanical properties of the steel wire not only decrease with the extension of the pitting corrosion length but also decrease with the increase of the pitting corrosion depth, and with the increase of the number of corrosion holes, the mechanical properties of the steel wire decrease more, but not significantly. Pitting corrosion results in a significant change in the cross-sectional geometry of the steel wire, from circular to noncircular. Therefore, compared with uniform corrosion, the mechanical properties of the steel wire decrease more, and the brittle fracture mechanism also changes, which originates from the corrosion holes on the surface of the steel wire.

5.1. Influence of Pitting Depth on Mechanical Properties of Steel Wire. The evolution law of mechanical properties of steel wire under different depth pitting corrosion conditions is shown in Figures 11 and 12.

Table 2: Ultimate strain of steel wire under pitting corrosion at different positions.

Corrosion time (h)	Pitting length (mm)	Pitting depth (mm)	Ultimate strain under each working condition				
			A	B	C	D	Average value
100	1.25	0.038	0.046	0.046	0.045	0.044	0.045
	2.50	0.038	0.045	0.045	0.043	0.043	0.044
	3.75	0.038	0.045	0.044	0.042	0.042	0.043
	5.00	0.038	0.048	0.048	0.047	0.045	0.047
200	1.25	0.077	0.042	0.040	0.050	0.038	0.043
	2.50	0.077	0.040	0.039	0.037	0.035	0.038
	3.75	0.077	0.039	0.038	0.036	0.034	0.037
	5.00	0.077	0.047	0.045	0.043	0.037	0.043
300	1.25	0.115	0.038	0.038	0.034	0.033	0.036
	2.50	0.115	0.036	0.035	0.032	0.031	0.034
	3.75	0.115	0.035	0.034	0.031	0.030	0.033
	5.00	0.115	0.045	0.039	0.035	0.031	0.038
400	1.25	0.154	0.033	0.033	0.030	0.029	0.031
	2.50	0.154	0.033	0.031	0.028	0.027	0.030
	3.75	0.154	0.033	0.031	0.028	0.026	0.030
	5.00	0.154	0.041	0.035	0.031	0.025	0.033
500	1.25	0.192	0.031	0.031	0.026	0.025	0.028
	2.50	0.192	0.030	0.028	0.024	0.022	0.026
	3.75	0.192	0.030	0.027	0.024	0.021	0.026
	5.00	0.192	0.038	0.032	0.028	0.021	0.030
600	1.25	0.230	0.028	0.028	0.024	0.022	0.026
	2.50	0.230	0.028	0.027	0.021	0.019	0.024
	3.75	0.230	0.028	0.026	0.021	0.018	0.023
	5.00	0.230	0.036	0.029	0.024	0.018	0.027
700	1.25	0.269	0.027	0.025	0.022	0.020	0.024
	2.50	0.269	0.026	0.024	0.020	0.017	0.022
	3.75	0.269	0.027	0.024	0.020	0.016	0.022
	5.00	0.269	0.034	0.026	0.020	0.016	0.024
800	1.25	0.307	0.029	0.028	0.020	0.019	0.024
	2.50	0.307	0.031	0.028	0.019	0.016	0.024
	3.75	0.307	0.032	0.025	0.018	0.014	0.022
	5.00	0.307	0.032	0.023	0.018	0.013	0.022

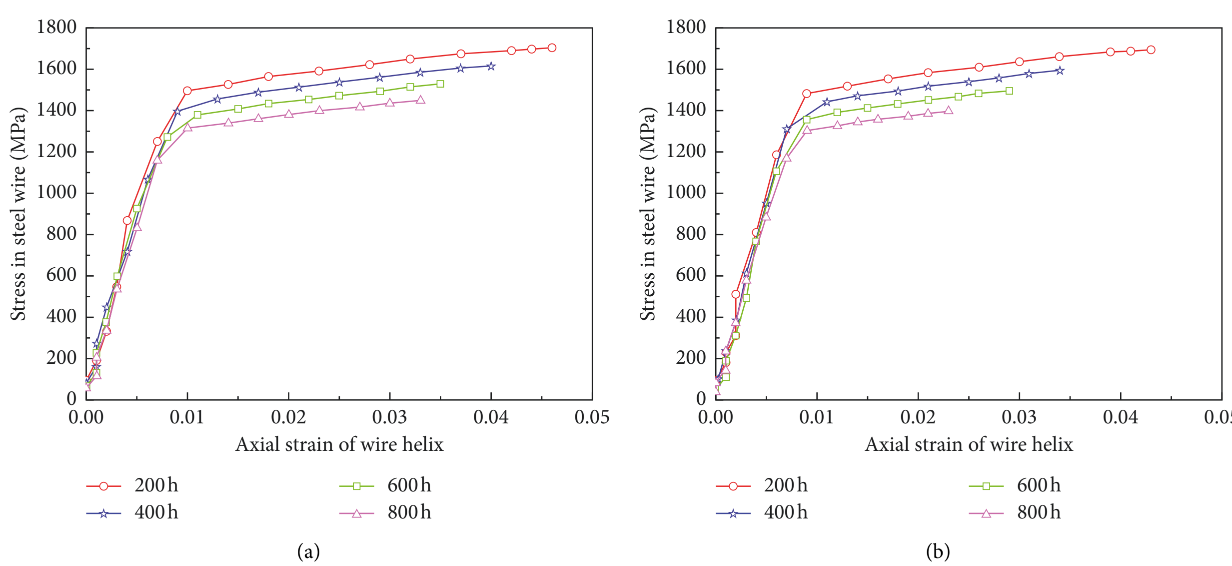

Figure 11: Continued.

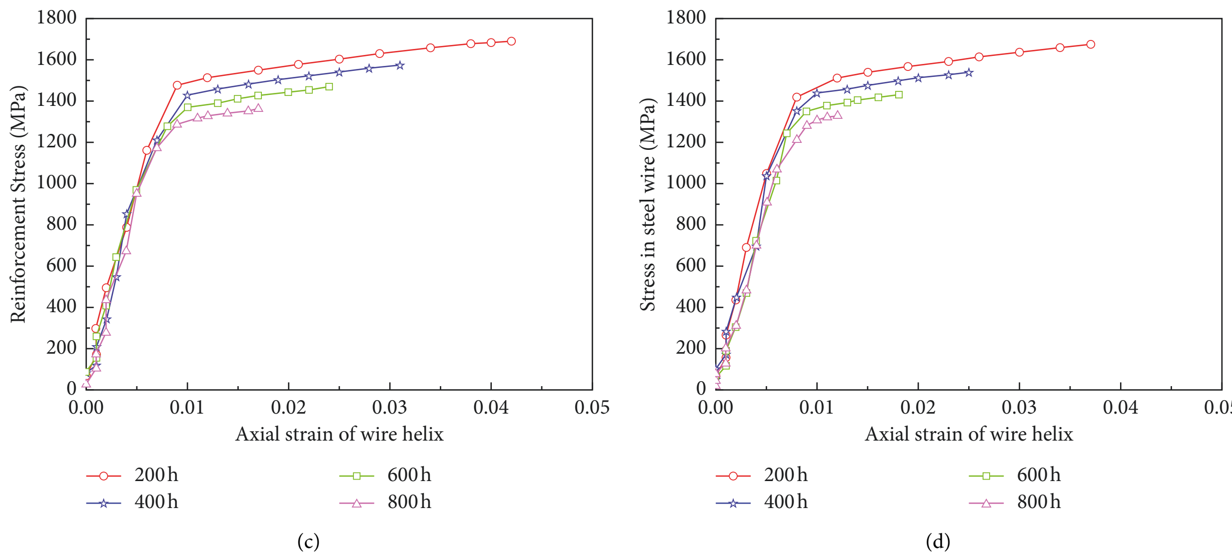

Figure 11: Changes in mechanical properties of steel wire at different depths of pitting corrosion.

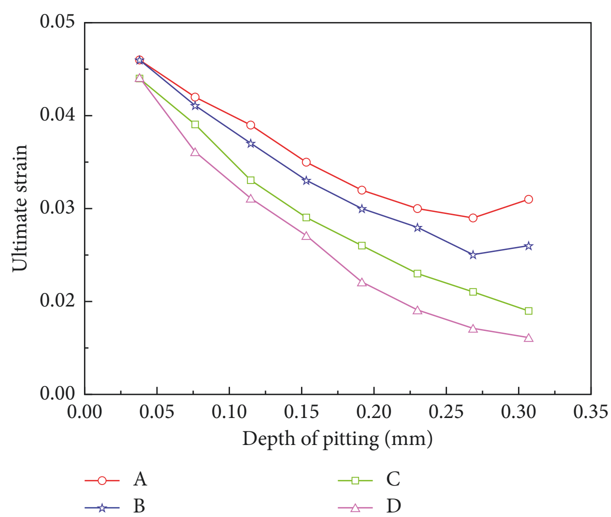

Figure 12: Influence of pitting depth on the ultimate strain of steel wire.

It can be seen from the figures that when the pitting corrosion depth of the steel wire gradually develops from 0.03848 mm (100 h) to 0.3078 mm (800 h), the ultimate strain, strength, and stiffness of the steel wire are reduced to varying degrees. When the steel wire has one corrosion hole, the impact of pitting depth on the mechanical properties of the steel wire is relatively minimal; when there are two corrosion holes, the effect is centered, but the closer the corrosion holes are, the greater the impact is; when there are three corrosion holes, the impact is the greatest.

Under the same corrosion depth, pitting corrosion has a greater impact on the mechanical properties of the steel wire than uniform corrosion. At the same time, with the increase of pitting corrosion depth, the cross-sectional geometry of the steel wire changes greatly, and the brittle fracture mechanism of the steel wire changes: the fracture originates from the deepest corrosion hole on the surface of the steel wire.

5.2. Effect of Pitting Corrosion Length on Mechanical Properties of Steel Wire. In the case of pitting corrosion of different lengths, the evolution law of the mechanical properties of the steel wire is shown in Figures 13 and 14.

It can be seen from the figures that when the uniform corrosion length of the steel wire gradually develops from 1.25 mm to 5.00 mm, the ultimate strain, strength, and stiffness of the steel wire all have a certain amount of reduction, but it is not significant. Compared with the corrosion conditions A~D, the effect of pitting corrosion length on the mechanical properties of the steel wire has little difference. At the same time, the impact of the pitting corrosion length on the mechanical properties of the steel wire is much smaller than that of the pitting corrosion depth, which indicates that the pitting corrosion depth and location of the steel wire are much smaller. The impact on its brittle fracture is obvious.

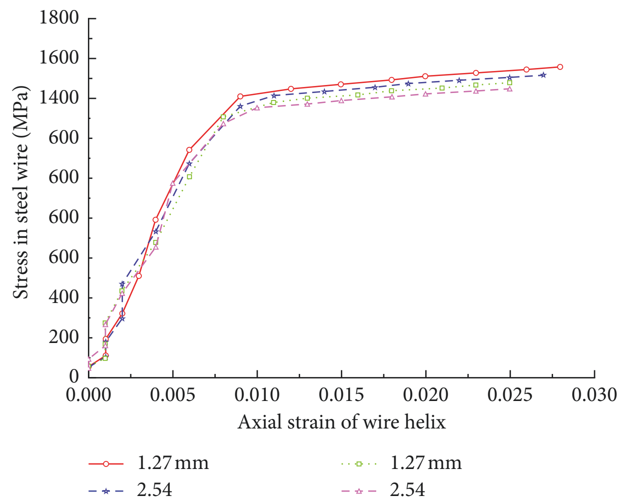

Figure 13: Influence of pitting corrosion length on mechanical properties of steel wire (condition D).

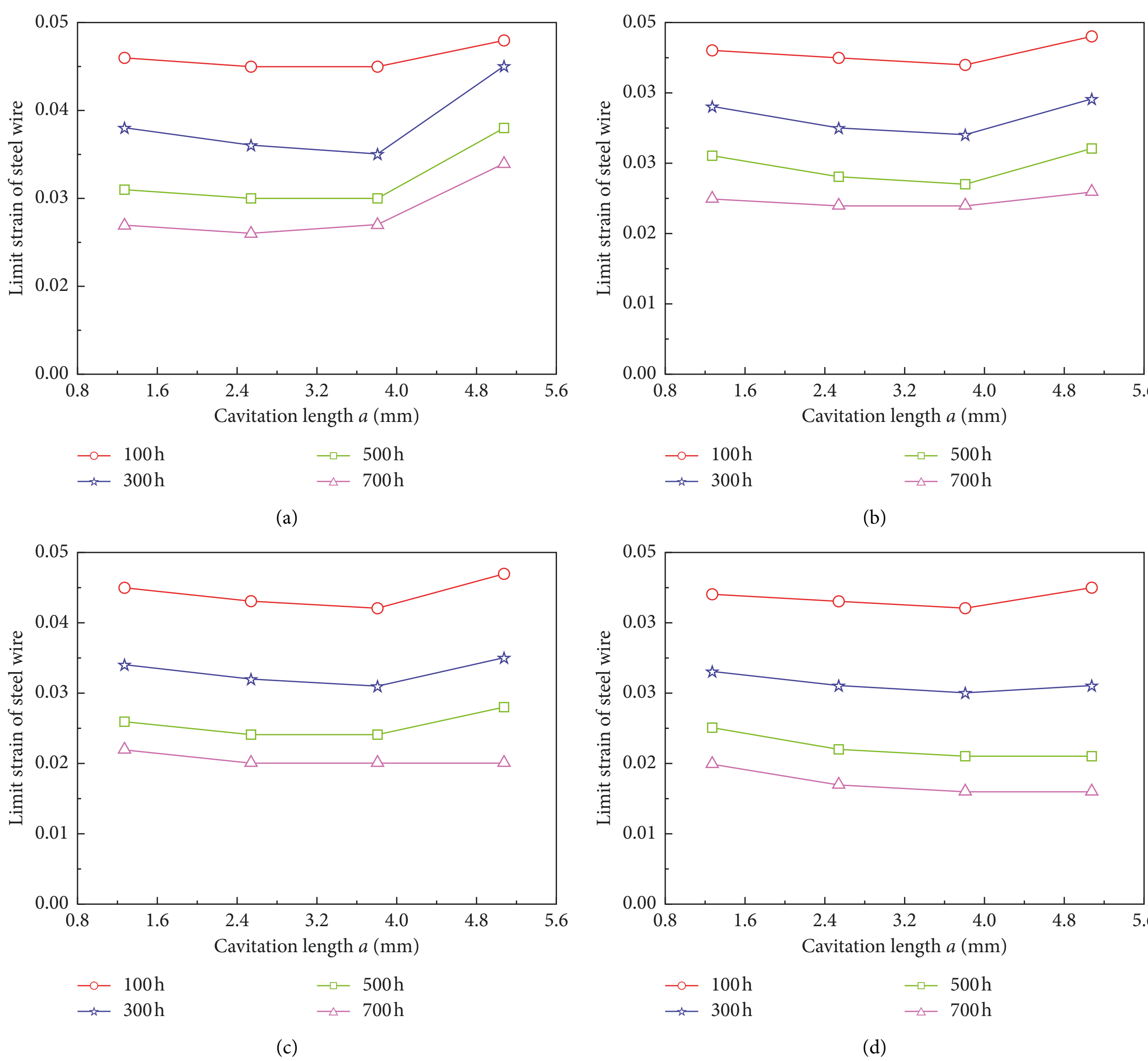

Figure 14: Influence of pitting length on the ultimate strain of steel wire under different working conditions.

6. Conclusion

In this paper, based on the ANSYS finite element platform, the degradation law of the mechanical properties of the hanger steel wire with the degree of corrosion is analyzed. Based on the simulations, we draw the following conclusions:

(1) The geometry of the cross section of the steel wire is one of the key factors leading to the degradation of the mechanical properties of the steel wire. The change of the geometry of the cross section of the steel wire is mainly determined by the degree of uniform corrosion and pitting corrosion.

(2) When the steel wire is in good condition, the fracture type is cup-conical fracture; in the case of uniform corrosion, the fracture originates in the center of the wire and then expands outward, with the fracture retaining a cup-conical shape; in pitting corrosion, the fracture originates from the corrosion hole on the surface of the steel wire.

(3) With the increase of the uniform corrosion depth and length, the ultimate strain of the steel wire decreases, but its strength and stiffness are not significantly reduced; with the increase of the depth and length of the pitting corrosion, the ultimate strain, strength, and stiffness of the steel wire are reduced to different degrees. The effect of uniform corrosion is more pronounced.

(4) The position and number of corrosion holes have a certain influence on the mechanical properties of the degraded steel wire: when the steel wire has one corrosion hole, the impact of pitting corrosion on the mechanical properties of the steel wire is relatively small; when there are two corrosion holes, the effect is centered, and the closer the two corrosion holes, the greater the impact; when there are three corrosion holes, the impact is the greatest.

Appendix

A

The line segment OA in the figure is parallel to BC, and the meanings of the symbols are as follows.

ε_e: ultimate elastic strain
ε_y: yield strain
ε_u: ultimate strain
ε_f: failure strain
F_y: yield bearing capacity of steel wire
F_u: ultimate bearing capacity of steel wire
E: elastic modulus of steel wire.

Data Availability

The experimental data used to support the findings of this study are included within the article.

Conflicts of Interest

The authors declare that there are no conflicts of interest regarding the publication of this paper.

References

[1] C. Liu, Y. Wang, X. Hu, Y. Han, X. Zhang, and L. Du, "Application of GA-BP neural network optimized by Grey Verhulst model around settlement prediction of foundation pit," *Geofluids*, vol. 2021, Article ID 5595277, 16 pages, 2021.

[2] A. Carpinteri and R. Brighenti, "Part-through cracks in round bars under cyclic combined axial and bending loading," *International Journal of Fatigue*, vol. 18, no. 1, pp. 33–39, 1996.

[3] P. Zhang, D. F. Zhang, Y. Yang et al., "A case study on intergrated modeling of spatial information of a complex geological body," *Lithosphere*, vol. 2022, no. s10, Article ID 2918401, 2022.

[4] L. Wang, X. Lu, L. Liu et al., "Influence of MgO on the hydration and shrinkage behavior of low heat Portland cement-based materials via pore structural and fractal analysis," *Fractal and Fractional*, vol. 6, no. 1, p. 40, 2022.

[5] L. Han, L. Wang, X. Ding, H. Wen, X. Yuan, and W. Zhang, "Similarity quantification of soil parametric data and sites using confidence ellipses," *Geoscience Frontiers*, vol. 13, no. 1, Article ID 101280, 2022.

[6] J. I. Xiao-Ming and L. Wei, "Review of research on instability failure mechanism and stability control of tunnel surrounding rock in water-bearing sandy ground," *Rock and Soil Mechanics*, vol. 30, 2009.

[7] Z. Liu, C. Y. Zhou, and M. Fang, "Failure criterion and deformation instability evaluation analysis of a tunnel by nonlinear dynamics," *Yantu Lixue/Rock and Soil Mechanics*, vol. 31, no. 12, pp. 3887–3893, 2010.

[8] L. Fang and D. Shao, "Application of long short-term memory (LSTM) on the prediction of rainfall-runoff in karst area," *Frontiers in Physics*, p. 685, 2022.

[9] B. Chen, W. Zhao, Y. Wang, and S. Xie, "Finite element analysis of cervical spine plate using double cage fusion," in *Proceedings of the 4th International Conference on Bioinformatics and Biomedical Engineering*, pp. 1–5, IEEE, Chengdu, China, July2010.

[10] J. P. Wang, Z. C Zhong, C. K Cheng et al., "Finite element analysis of the spondylolysis in lumbar spine," *Bio-Medical Materials and Engineering*, vol. 16, no. 5, pp. 301–308, 2006.

[11] J. Llorca and V. Sánchez-Gálvez, "Fatigue limit and fatigue life prediction in high strength cold drawn eutectoid steel wires," *Fatigue and Fracture of Engineering Materials and Structures*, vol. 12, no. 1, pp. 31–45, 1989.

[12] N. Couroneau and J. Royer, "Simplifying hypotheses for the fatigue growth analysis of surface cracks in round bars," *Computers & Structures*, vol. 77, no. 4, pp. 381–389, 2000.

[13] X. Zheng, X. Xie, and X. Li, "Experimental study and residual performance evaluation of corroded high-tensile steel wires," *Journal of Bridge Engineering*, vol. 22, no. 11, p. 04017091, 2017.

[14] Z. Dou, S. Tang, X. Zhang et al., "Influence of shear displacement on fluid flow and solute transport in a 3D rough fracture," *Lithosphere*, vol. 2021, 2021.

[15] D. Chen, H. Chen, W. Zhang, J. Lou, and B. Shan, "An analytical solution of equivalent elastic modulus considering confining stress and its variables sensitivity analysis for fractured rock masses," *Journal of Rock Mechanics and Geotechnical Engineering*, 2021.

[16] C. Cao, W. Zhang, J. Chen, B. Shan, S. Song, and J. Zhan, "Quantitative estimation of debris flow source materials by integrating multi-source data: a case study," *Engineering Geology*, vol. 291, Article ID 106222, 2021.

[17] G. Li, Y. Hu, S.-m. Tian, M. weibin, and H.-l. Huang, "Analysis of deformation control mechanism of prestressed anchor on jointed soft rock in large cross-section tunnel," *Bulletin of Engineering Geology and the Environment*, vol. 80, no. 12, pp. 9089–9103, 2021.

[18] C. Liu, L. Du, X. Zhang, Y. Wang, X. Hu, and Y. Han, "A new rock brittleness evaluation method based on the complete stress-strain curve," *Lithosphere*, vol. 2021, Article ID 4029886, 2021.

[19] J. Toribio, J. Matos, and B. González, "Micro-and macro-approach to the fatigue crack growth in progressively drawn pearlitic steels at different R-ratios," *International Journal of Fatigue*, vol. 31, no. 11-12, pp. 2014–2021, 2009.

[20] A. Carpinteri, R. Brighenti, and A. Spagnoli, "Part-through cracks in pipes under cyclic bending," *Nuclear Engineering and Design*, vol. 185, no. 1, pp. 1–10, 1998.

[21] J. Toribio and M. Toledano, "Fatigue and fracture performance of cold drawn wires for prestressed concrete," *Construction and Building Materials*, vol. 14, no. 1, pp. 47–53, 2000.

[22] B. Yuan, Z. Li, Z. Zhao, H. Ni, Z. Su, and Z. Li, "Experimental study of displacement field of layered soils surrounding laterally loaded pile based on transparent soil," *Journal of Soils and Sediments*, vol. 21, no. 9, pp. 3072–3083, 2021.

[23] B. Yuan, Z. Li, Y. Chen et al., "Mechanical and microstructural properties of recycling granite residual soil reinforced with glass fiber and liquid-modified polyvinyl alcohol polymer," *Chemosphere*, vol. 286, Article ID 131652, 2022.

[24] S. M. Elachachi, D. Breysse, S. Yotte, and C. Cremona, "A probabilistic multi-scale time dependent model for corroded structural suspension cables," *Probabilistic Engineering Mechanics*, vol. 21, no. 3, pp. 235–245, 2006.

[25] J. Xu, *Damage Evolution Mechanism and Remained Service Lives Evaluation of Stayed Cables*, Tongji University, Shanghai, China, 2006.

[26] J. Lemaitre and J.-L. Chaboche, *Mechanics of Solid Materials*, Cambridge University Press, Chennai, 1994.

[27] X. Li, Q. Li, Y. Hu et al., "Study on three-dimensional dynamic stability of open-pit high slope under blasting vibration," *Lithosphere*, vol. 2021, no. Special 4, p. 6426550, 2022.

[28] C. Zhu, M. Karakus, M. He et al., "Volumetric deformation and damage evolution of Tibet interbedded skarn under multistage constant-amplitude-cyclic loading," *International Journal of Rock Mechanics and Mining Sciences*, vol. 152, Article ID 105066, 2022.

[29] Y. Wang, H. Yang, J. Han, and C. Zhu, "Effect of rock bridge length on fracture and damage modelling in granite containing hole and fissures under cyclic uniaxial increasing-amplitude decreasing-frequency (CUIADF) loads," *International Journal of Fatigue*, vol. 158, Article ID 106741, 2022.

[30] Y.-q. Su, F.-q. Gong, S. Luo, and Z.-x. Liu, "Experimental study on energy storage and dissipation characteristics of granite under two-dimensional compression with constant confining pressure," *Journal of Central South University*, vol. 28, no. 3, pp. 848–865, 2021.

[31] Z.-j. Wu, Z.-y. Wang, L.-f. Fan, L. Weng, and Q.-s. Liu, "Micro-failure process and failure mechanism of brittle rock under uniaxial compression using continuous real-time wave velocity measurement," *Journal of Central South University*, vol. 28, no. 2, pp. 556–571, 2021.

[32] S. Maleki and S. Bagheri, "Behavior of channel shear connectors, Part II: analytical study," *Journal of Constructional Steel Research*, vol. 64, no. 12, pp. 1341–1348, 2008.